

# Finding stable minima using a nudged-elastic-band-based optimization scheme

J. A. Hirschfeld\*

*Forschungszentrum Jülich, Institute for Advanced Simulation (IAS-1), 52425 Jülich, Germany*

H. Lustfeld

*Forschungszentrum Jülich, Peter Grünberg Institute (PGI-1), 52425 Jülich, Germany*

(Received 13 March 2012; revised manuscript received 8 May 2012; published 29 May 2012)

Optimization is essential in many scientific and economical areas, but it is often too complex to be tackled by simple straightforward calculations or by trial and error. Two well-known methods to find low-lying minima in such complex systems are simulated annealing and the genetic algorithm. In these methods artificial fluctuations control the probability of the system to overcome a local minimum having a certain depth. Here we present a complementary scheme that is based on the nudged-elastic-band method ordinarily used to find saddle points and we apply the scheme to find the most stable isomers of the phosphorus  $P_4$ ,  $P_8$  molecules and the corresponding molecules of  $As_n$ ,  $Sb_n$ , and  $Bi_n$  ( $n = 4, 8$ ) in the framework of the density functional theory. In the case of  $n = 8$  we have found stable and metastable configurations, some of which are new and have similar energies. As a by-product we obtained an upper bound for the energy barriers between these configurations.

DOI: [10.1103/PhysRevE.85.056709](https://doi.org/10.1103/PhysRevE.85.056709)

PACS number(s): 02.60.Pn, 31.50.Bc, 31.15.E-, 33.15.Hp

## I. INTRODUCTION

Finding new stable configurations is important for the fundamental understanding of material properties, for developing new stable materials with novel properties, and, in general, whenever optimization is necessary, e.g., in engineering and economics. However, the optimization problem can become very complex due to many local minima in a high dimensional phase space. Simple minimum search procedures often fail, and sophisticated optimization schemes are required. Many of these rest on simulated annealing [1] and the genetic algorithm [2].

In simulated annealing the annealing process of condensed matter is imitated to find stable configurations. This is achieved by introducing a temperature parameter  $T$  controlling temperature fluctuations. At high  $T$  the fluctuations are large and it is possible to overcome large energy barriers between local minima. By decreasing  $T$  the fluctuations are diminished and lead to a more stable minimum than can be found with simple search methods. The extent of application possibilities are immense for simulated annealing. Some of many applications are finding stable isomers of phosphorus clusters [3], designing heterogeneous catalytic reactors [4], three-dimensional face recognition [5], the optimization of electric discharge machining [6], the inverse calculation of experimental scattering data [7], or a search algorithm for structures and substructures of proteins in a database [8]. A similar method is the simulated quenching, which has been applied for example to the design of optical elements [9].

In the genetic algorithm a set (population) of different configurations is considered. In addition to small random variations of the configurations (mutations), the properties of the most successful states are melded to find even more stable ones, thus imitating inheritance in genetics. Also, the genetic algorithm has been used for many different applications: finding of Sb clusters [10], finding stable alloys based

on density functional theory (DFT) out of 19016 possible combinations [11], or finding crystal structures in constrained systems [12]. Although simulated annealing and the genetic algorithm address the problem of local minima, there can be no guarantee that the configuration obtained by these methods is the global minimum. Therefore, there is a need for other, complementary methods.

In this paper, we propose a scheme to find low-lying minima in complex systems that employs the nudged-elastic-band (NEB) method [13–15]. The key points of our method are (a) due to the band not only one single point of the phase space is selected but a series of points (images) that communicate with each other, (b) local minima are easily overcome by using the so-called nudging of images, and (c) randomness can be included by using different, random starting positions, while at the same time increasing knowledge during the search process can be incorporated when selecting configurations as new starting points in phase space.

In the next section we emphasize the features of the NEB method that make it useful for our purpose, i.e., by avoiding irrelevant local minima. In Sec. III, we present the algorithm and, in Sec. IV, we show that (i) the NEB-based optimizer reproduces well-known minima of the  $P_4$  cluster [16] and (ii) by applying it to the  $P_8$  cluster [17–19] we find a new most stable isomer. We also apply our method to find the most stable configuration of chemically similar compounds in the same main group, i.e.,  $As_n$ ,  $Sb_n$ , and  $Bi_n$  ( $n = 4, 8$ ). As a by-product we obtain an upper bound for the energy barriers between these configurations. All calculations are done in the framework of DFT.

## II. NEB IN THE NEIGHBORHOOD OF A MINIMUM

Any scheme searching for global minima can succeed only if it (i) can overcome local minima and (ii) can find the low-lying minima. We now show that appropriate use of the NEB method can do both, although it was not developed for this purpose. Images of the system are connected by straight lines

\*j.hirschfeld@fz-juelich.de

starting from a first image  $i = 1$  up to the last image  $i = N$ . The band constructed in this way moves through the phase space, while three kinds of forces act [13] upon each image ( $1 < i < N$ ) at position  $\mathbf{R}_i$ ,

$$\begin{aligned} \mathbf{F}_i &= \mathbf{F}_{i1} + \mathbf{F}_{i2} + \mathbf{F}_{i3} \\ &= -\nabla E(\mathbf{R}_i) + \hat{\boldsymbol{\tau}}_i \hat{\boldsymbol{\tau}}_i \cdot \nabla E(\mathbf{R}_i) + \hat{\boldsymbol{\tau}}_i \alpha_i. \end{aligned} \quad (1)$$

$E_i$  is the energy and  $\mathbf{F}_{i1}$ , the force acting on each image due to the local potential, is also used in the drag method [14].  $\mathbf{F}_{i2}$  and  $\mathbf{F}_{i3}$  are, however, special to the NEB method and are quite important.  $\mathbf{F}_{i2}$  cancels the force  $\mathbf{F}_{i1}$  along the direction of the normalized “tangent” vector

$$\hat{\boldsymbol{\tau}}_i = \boldsymbol{\tau}_i / |\boldsymbol{\tau}_i| \quad (2)$$

of the band and replaces it by  $\mathbf{F}_{i3}$ , an artificial spring force in the same direction, obtained from

$$\alpha_i = k (|\mathbf{R}_{i+1} - \mathbf{R}_i| - |\mathbf{R}_i - \mathbf{R}_{i-1}|), \quad (3)$$

with the spring constant  $k$ .  $\boldsymbol{\tau}_i$  is obtained from the requirement that the additional terms  $\mathbf{F}_{i2}$  and  $\mathbf{F}_{i3}$  must not change the length of the band, yielding [15]

$$\boldsymbol{\tau}_i = \frac{\mathbf{R}_i - \mathbf{R}_{i-1}}{|\mathbf{R}_i - \mathbf{R}_{i-1}|} + \frac{\mathbf{R}_{i+1} - \mathbf{R}_i}{|\mathbf{R}_{i+1} - \mathbf{R}_i|}. \quad (4)$$

This construction of  $\mathbf{F}_i$  has distinct consequences for images within the range of a minimum, which depend on the choice of the parameter  $k$  and distance between two successive images. Using the total length of the band  $L_{\text{band}}$ , the average distance  $S$  is obtained by

$$S = L_{\text{band}} / (N - 1). \quad (5)$$

Let us first turn to the parameter  $k$ . As shown in Fig. 1 an image  $i$  can pass an equipotential surface around an attracting minimum only if

$$|\mathbf{F}_{i1}| \sin^2(\gamma) < |\mathbf{F}_{i3}| \cos(\gamma). \quad (6)$$

Here  $\gamma$  is the angle between the normal of the equipotential surface and the tangent vector  $\hat{\boldsymbol{\tau}}_i$ .  $\gamma$  can assume any value in the

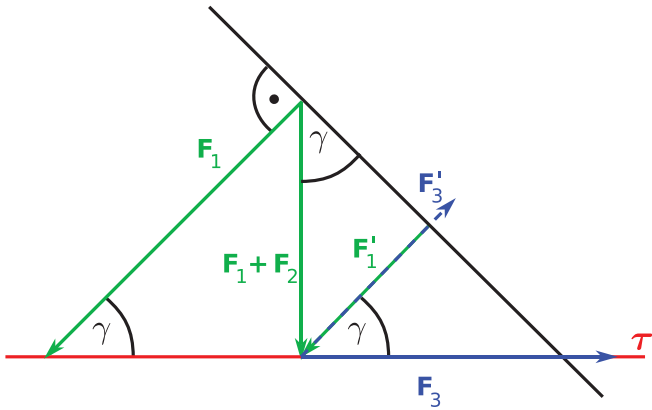


FIG. 1. (Color online) Passing of an equipotential surface: the force  $\mathbf{F}_1$  is perpendicular to the equipotential surface (black).  $\gamma$  is the angle between  $\mathbf{F}_1$  and the tangent  $\boldsymbol{\tau}$ .  $\mathbf{F}'_1$  is the resulting force component pulling the image toward the minimum.  $\mathbf{F}'_3$  is the component of the artificial spring force pushing the image out of the attractor. If  $|\mathbf{F}'_1| < |\mathbf{F}'_3|$ , the image will pass the equipotential surface, i.e., depart from the minimum.

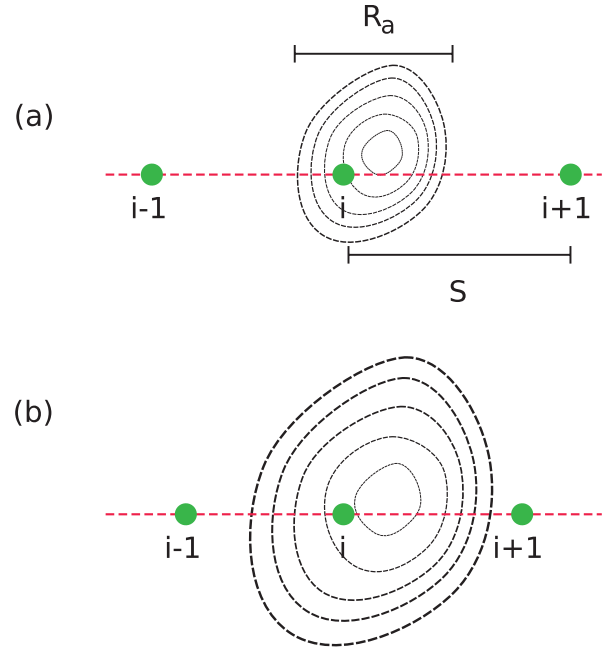


FIG. 2. (Color online) Sketch of the band in the neighborhood of a minimum. In (a)  $S > R_a$ ; in (b)  $S < R_a$ . In both cases image  $i$  can escape from the range of attraction if, e.g., image  $(i + 2)$  nudges sufficiently to the right. In (a) the band will then escape from the minimum; in (b) it will not.

interval  $]-90^\circ, +90^\circ[$ , and  $\sin^2(\gamma) < 0.1$  for  $|\gamma| \lesssim 20^\circ$ . If  $k$  is not small, the probability of a trapped image escaping from a local minimum is not small. On the other hand, the probability vanishes for  $k \rightarrow 0$  and thus the band cannot escape the range of attraction  $R_a$  of the minimum.

If  $k$  is not too small, the motion of the images can easily be understood, since the distances between all images are approximately equal and given by  $S$ . Figure 2 shows a snapshot where image  $i$  is in the range of attraction  $R_a$  of a local minimum. If the image  $(i + 2)$  is nudged to the right, for example, all the images  $m < (i + 2)$  will move along their tangent vectors  $\hat{\boldsymbol{\tau}}_m$ , and the image  $i$  can escape easily from the local minimum. At the same time, however, image  $(i - 1)$  has moved closer to the local minimum. If  $S \gtrsim R_a$ , image  $(i - 1)$  will not enter the range of attraction, and the band has escaped from the local minimum. For  $S \lesssim R_a$ , image  $(i - 1)$  has a high probability of entering the range of attraction. The net result is that the image  $i$  has escaped from the local minimum, whereas the band has not.

As  $S$  decreases, the probability increases that the band, once in the range of a local minimum, does not escape. For  $S \rightarrow 0$ , this is true for all  $k$ , as the following argument shows: for  $S \rightarrow 0$  the band becomes a smooth curve, the vectors  $\hat{\boldsymbol{\tau}}_i$  become the genuine tangent vectors of the curve, and  $\mathbf{F}_{i3}$  cannot change the shape of the band. If the band now enters the range of attraction of a local minimum,  $\mathbf{F}_{i1} + \mathbf{F}_{i2}$ , being orthogonal to the curve, will pull the band in the direction of the minimum (Fig. 3). The only effect of  $\mathbf{F}_{i3}$  is to move images along the band, so that some images may escape from the local minimum. But this is irrelevant because the band remains captured.

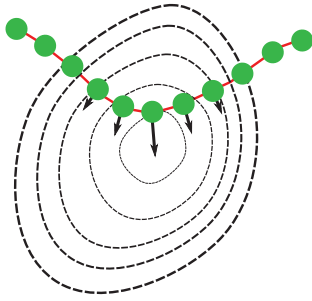


FIG. 3. (Color online) If  $S \rightarrow 0$ ,  $\mathbf{F}_{13}$  can only move the images along the band but cannot change its shape, and the band cannot escape from the minimum.

To summarize, the escape of the band from a minimum depends on (i) the value of the parameter  $k$ , (ii) the value of the length  $S$ , and (iii) the nudging process. The corresponding algorithm will now be described.

### III. THE ALGORITHM

The NEB method, introduced to change saddle-point problems into minimum-finding problems, is used here to find the stable configurations of molecules which requires modification. In the original method, the first and the last image of the band are usually relaxed to ensure that the bottom of the potential well is reached. In our case, however, it is not necessary to start or end in a minimum, and the first and last image of the band can be chosen (i) as random configurations (ii) from known stable or metastable configurations of this or related compounds (iii) exploiting knowledge from previous calculations. However, the first and the last image of the band should be distinctly different. This can be achieved by choosing at least one configuration randomly or by starting with two states with quite different symmetries, as in a molecule. Known configurations can be included as the first or last image of the band. After specifying these images the band is created by  $(N - 2)$  additional images.  $N$  determines  $S$  [see Eq. (5)], the mean distance between the images, and hence the minima that can be overcome, because their range of attraction  $R_a \lesssim S$ . Assuming that  $R_a$  of the stable state in question is of the same order of magnitude as that of known stable states of this or similar systems one can choose  $N$  correspondingly or start with a small value.

The motion of the band occurs in cycles in each of which the band is first relaxed as in a typical NEB for  $n_r$  ionic relaxation steps following Eq. (1). Equation (3) implies that the images do not relax independently, but “nudge” each other and begin to scan an area around the initial band. Nudging is crucial in our method and is implemented by moving, removing, or adding images after the  $n_r$  relaxation steps: either the image with highest energy is removed and a new one is set to the position with lowest energy in the band (even cycles), or a new image is set at the lowest point of the band, increasing the number of images in the band (odd cycles). A different situation arises if neighboring images relax to degenerate minima that transform into each other by translations or rotations of the system. If there are images located in such a minimum, they usually cannot escape and even attract more images into it, which makes them inactive for the optimization process. All but one of these degenerate images are discarded, and a new image is generated at the position of the band with lowest energy. These manipulations (adding, moving, and removing images) end a cycle and may lead to a new  $N$ . The steps executed in the ordinary use of NEB are contrasted in Table I to the steps taken in the new optimization scheme.

The nudging dynamics is retained from cycle to cycle, enabling the images to overcome local minima along the tangential direction  $\hat{\tau}_i$  independent of the barrier height, and to relax perpendicular to  $\hat{\tau}_i$  toward the global minimum (cf. Fig. 2).

$S$  is by no means a constant in an optimization run, even for constant  $N$ . In fact, due to the relaxation of the band perpendicular to  $\hat{\tau}_i$  the length of the band varies and fluctuates. At the beginning of an optimization run,  $S$  can increase even if the number of images increases. This effect is certain to occur if a straight line connects the first with the last image at the beginning of an optimization run, and relaxation can only prolong the band. When the band approaches more relaxed states, the addition of images will reduce  $S$ , but fluctuations of  $S$  remain part of the nudging process. This does not matter, at least as long as  $S$  does not change by an order of magnitude. Moreover, the reduction of  $S$  below a threshold  $S_{\text{conv}}$  appears to be unnecessary as long as one can estimate  $R_a$  of the stable state.

An alternative way to reduce the chance to escape local minima is given by decreasing  $k$  throughout the optimization process [Eq. (6)]. Inspired by simulated annealing, this

TABLE I. Comparing the steps of the classic NEB and our optimization method (possible changes of  $k$  have not been entered in the table).

Step	Classic NEB	Optimization scheme
1	Choose initial and final configuration having barrier of interest in between	Choose initial and final configuration possibly randomly and sufficiently different
2	Relax initial and final state	
3	Interpolate between states	Interpolate between states
4	Use NEB to relax band to MEP until convergence	Use NEB to relax band for $n_r$ steps
5	Determine saddle point as the maximum of the MEP	Add image to low part of the band
6		Use NEB to relax band for $n_r$ steps
7		Delete image with highest energy and add image to low part of the band
8		Go back to step 4

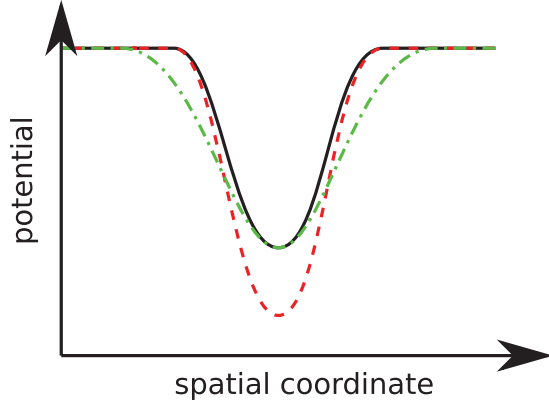


FIG. 4. (Color online) Different types of minima have distinct consequences in simulated annealing and in our method.

reduction could follow an exponential law, e.g., for the  $k$  value of the  $j$ th cycle,

$$k_j = k_{\text{init}} \exp[-A(j-1)], \quad (7)$$

with a scaling factor  $A$ . In this way  $k$  goes to zero as  $j$  increases. Such procedures are necessary if there are limits on the number of images. It is important to point out that the reduction of  $k$  can be achieved in different manners and the choice of exponential decay implies by no means that  $k$  corresponds to the temperature parameter of simulated annealing. In systems of modest size, we found that it was more efficient to increase the numbers of images. We note that it may be desirable to stabilize or destabilize parts of the band, and this can be achieved by locally decreasing or increasing the  $k$  values.

In simulated annealing the probability that a point in phase space escapes from a minimum depends on its depth and the temperature  $T$ . In our scheme the probability for the band to escape from a minimum depends on its range of attraction  $R_a$ ,  $k$ , and  $S$ . The consequences of this difference become clear when we examine how the methods behave in the vicinity of various types of minima (Fig. 4). In simulated annealing the chance to escape the basin of attraction of the minimum in the dashed (red) lined potential is lower than in the black one, while there is little difference between the minima in the solid (black) lined and the dash-dotted (green) potential. The larger attractor size means that the opposite is true for the NEB-based optimizer. The minimum in the dash-dotted (green) potential is harder to escape from than from the one in the solid lined (black) potential, while the chances to escape from the minimum in the deeper (red) potential is equal to the one of the solid lined (black) potential. This distinction shows that our scheme complements other procedures. It should be mentioned that—as in any NEB procedure—the method provides an upper bound for the stability of the obtained minimum by providing the barrier along the final band.

With our method it is also possible to obtain metastable configurations of high energy but the optimization must be executed slightly differently: the newly added images are not set to the lowest energy of the band but are randomly distributed over the band.

In this paper we restrict ourselves to molecular applications and present examples to show the effectiveness and power

of the algorithm, but we emphasize that our scheme can be applied to quite different optimization problems.

#### IV. APPLICATIONS

The algorithm has been tested for simple molecules, e.g.,  $\text{H}_2\text{O}$  starting from an oxygen atom and a hydrogen molecule, where it is easy to find the minimum. Further tests have been carried out with more complex molecules: the  $P_4$  and  $P_8$  clusters and the corresponding molecules of arsenic, antimony, and bismuth. The  $P_4$  and the  $P_8$  molecules have been investigated by simulated annealing [3] and are satisfactory benchmark systems. We used the NEB method as implemented in the Vienna Ab Initio Simulation Package (VASP) without any modifications to the code. Except for the final relaxation to the minimum we used intermediate precision to achieve a high efficiency of the method. Increasing the precision further does not yield more information and only decreases the efficiency of the method.

##### A. Finding the most stable isomer of the $P_4$ cluster

The  $P_4$  cluster minimum has a steep basin of attraction, and it is not easy to find in simulated annealing. Typically a “roof” or “butterfly” structure is obtained by these methods. In our method the minimum can be found in a few cycles beginning from only one pair of starting configurations.

We start by randomly placing the four phosphorus atoms far from each other in a  $10 \text{ \AA} \times 10 \text{ \AA} \times 10 \text{ \AA}$  cell and initializing the last image  $i = N$  accordingly, noting that the images  $i = 1$  and  $i = N$  need to be quite different. The initial band is obtained by a linear interpolation connecting the initial images by a straight line in phase space. A Monkhorst-Pack  $K$ -point mesh of  $6 \times 6 \times 6$  and an energy cutoff of 270 eV has been used in the local density approximation (LDA). The electronic structure is calculated by including five valence electrons ( $3s^2 3p^3$ ). The ions are described by the projector augmented wave (PAW) method by Blöchl.

The initial band had a total length of  $L_{\text{band}} = 8.5 \text{ \AA}$  and we started with  $N = 4$  leading to an initial  $S_{\text{init}}$  value of  $1.7 \text{ \AA}$ . Although  $S_{\text{init}}$  was small in comparison to the expected range of attraction of the stable state  $R_a \approx 2.4 \text{ \AA}$ , the initial strong increase in  $S$  was accounted for in this way (after the first cycle,  $S = 2.2 \text{ \AA}$ ). In fact, with the convergence parameters  $n_r = 40$  and a constant  $k = -5 \text{ eV/\AA}^2$ , the most stable isomer of the  $P_4$  was found after 11 cycles (cf. Fig. 5). In the vicinity of the minimum we also found the “roof” structure.

##### B. Finding the most stable isomer of the $P_8$ cluster

In 1990 Jones and Hohl found a new most stable wedgelike ( $C_{2v}$  symmetry, Fig. 7) isomer of the  $P_8$  cluster [3]. Previously, it had been assumed that the high symmetry of the cubic structure would be favored.

We again set up the initial images with different random positions of all eight  $P$  atoms in both a  $10 \text{ \AA} \times 10 \text{ \AA} \times 10 \text{ \AA}$  computational cell using a  $6 \times 6 \times 6$   $K$ -point mesh and a  $12 \text{ \AA} \times 12 \text{ \AA} \times 12 \text{ \AA}$  computational cell using a  $3 \times 3 \times 3$   $K$ -point mesh with the same computational parameters as in the  $P_4$  calculation. Linear interpolation of the atomic positions was used to obtain the initial band. With  $S_{\text{init}} = 1.8 \text{ \AA}$  we

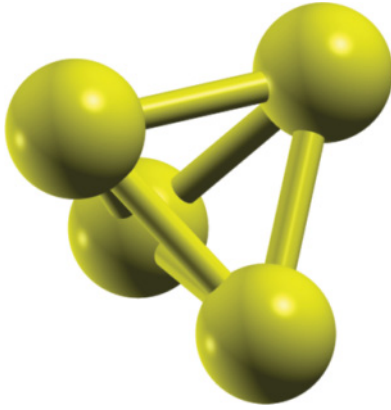


FIG. 5. (Color online) Optimized  $P_4$  cluster is a tetrahedron. (The atomic viewer XCrysDen has been used to create this picture [20].)

again started with a value smaller than the expected range of attraction,  $R_a \approx 3.5\text{--}5 \text{ \AA}$  to compensate the initial rise in  $S$  (cf. Fig. 6). In the small unit cell we reproduced the structure of Jones and Hohl, showing that our scheme can quickly reproduce well-known stable structures without including any assumptions. In the larger unit cell, however, we have obtained a configuration that is more stable than the previous one (cf. Fig. 7), namely a dimer of two  $P_4$  clusters. We have relaxed this structure with higher accuracy (900 eV energy cutoff in

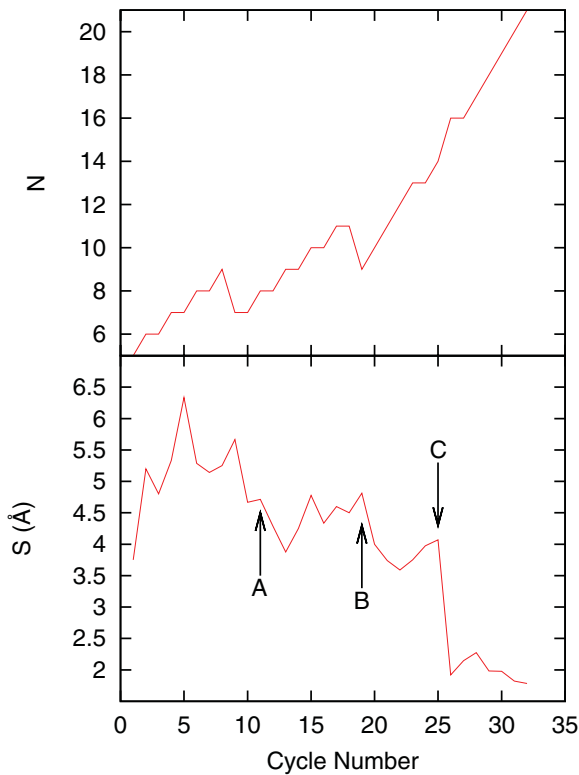


FIG. 6. (Color online) Development of  $S$  throughout the optimization of the  $P_8$  cluster as a function of the cycle number  $j$  (bottom panel) and the number of images in the band (top panel). At point A the dimer structure is observed the first time and persists as the lowest energy state through the following optimization. At point B and C the procedure was changed to reduce  $S$  further.

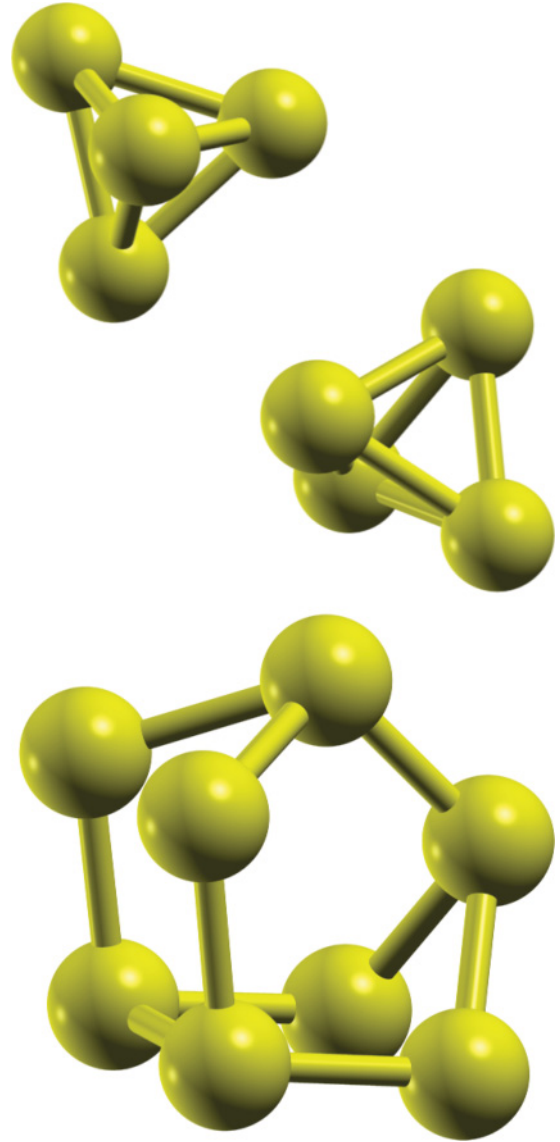


FIG. 7. (Color online) Low-energy states of the  $P_8$  cluster as found by our optimization scheme in DFT. Top: new dimer structure; bottom: wedgelike structure found by Jones and Hohl. (The atomic viewer XCrysDen has been used to create this picture [20].)

a  $20 \text{ \AA} \times 20 \text{ \AA} \times 20 \text{ \AA}$  computational cell), and the energies in LDA and in the generalized gradient approximation (GGA) using the Perdew-Burke-Ernzerhof (PBE) functional are given in Table II.

In Fig. 6, the development of  $S$  throughout the optimization of  $P_8$  in the  $12 \text{ \AA} \times 12 \text{ \AA} \times 12 \text{ \AA}$  unit cell is shown. Up to cycle 18, the algorithm led first to a strong increase of  $S$  and then

TABLE II. Energies (in eV) of the  $P_8$  cluster in different configurations.

	LDA	$E - 2E_{P_4}$	PBE	$E - 2E_{P_4}$
$2E_{P_4}$	-44.6964	0	-41.9968	0
$E_{\text{dim}}$	-44.9726	-0.2762	-42.0295	-0.0327
$E_{\text{wedge}}$	-44.8755	-0.1791	-41.5674	0.4294

to a decrease, until it oscillates around a value of about 4.5 Å. After the strong initial rise of  $S$ , the increase of  $L_{\text{band}}$  slows down and  $S$  is then decreased by the increase of images. To systematically decrease  $S$  further  $n_r$  is reduced to 10 and a new image added after every cycle. Since parts of the band always enlarge further in the phase space, this procedure will also approach its limit. If  $S$  has to be decreased further, another very efficient way is to remove unimportant high energy parts of the band, while redistributing the number of images removed over the remainder. This has been done at cycle 26 (cf. Fig. 6 point C) decreasing  $S$  from 4.0 Å to 1.9 Å, after which  $S$  does not change considerably. Although one has the option to decrease  $S$  systematically in this way, it was unnecessary in our cases, since the most stable isomer was typically found much faster (the lowest energy was found here after only 11 cycles).

The size of the computational cell affects the path of the optimization process and can affect the final structure. In the unit cell with a side length of 10 Å only the wedgelike structure was found. It is very hard to find the dimer structure in this cell, while in the 12 Å cell it was found quickly. The reason is the spatial extent of the structures. In the small cell the available phase space is too limited for the dimer structure to develop, while the more compact wedgelike structure can develop. Although the dimer structure is also more stable than the wedgelike configuration in the small cell, it cannot be found easily by the optimization scheme. A cell that is too large is also not ideal, since it is computationally more expensive and one or more atoms can be pushed away from the others by the artificial spring forces. Such atoms are unlikely to be incorporated into the molecule, but appropriate periodic boundary conditions can prevent this. The cell size (phase space) has to be experimented with in practice to discover new structures.

Due to the chemical similarity of the elements in the group 15 (except nitrogen) we also applied our optimization algorithm to the four and eight atom clusters of  $As$ ,  $Sb$ , and  $Bi$ . In these systems we also found either the wedgelike configuration or the dimer configuration. Also in these cases the cell-size dependence arises: the dimer structure was found only in large cells, while in the smaller cells only the wedgelike structure occurred. We compared the energies of the two stable isomers in all cases (cf. Table III) and found that  $As_8$  is also more stable in the dimer structure,  $Sb_8$  is more stable in the wedgelike structure, and in  $Bi_8$  both structures have nearly the same energy. In LDA, however, the wedgelike

TABLE III. Energies (in eV) of the  $Sb_8$ ,  $As_8$ , and  $Bi_8$  clusters in wedge and dimer configurations. All calculations are done in GGA-PBE with 600 eV energy cutoff and a  $k$ -point mesh of  $3 \times 3 \times 3$  in a cubic computational cell with the side length of 13 Å ( $As_8$ ), 14 Å ( $Sb_8$ ), or 20 Å ( $Bi_8$ ).

	$As_8$	$Sb_8$	$Bi_8$
$E_{\text{dim}}$	-35.878	-30.681	-29.829
$E_{\text{wedge}}$	-35.703	-30.734	-29.827
$E_{\text{dim}} - E_{\text{wedge}}$	-0.175	0.053	-0.002

TABLE IV. Energies (in eV) of the  $Sb_8$ ,  $As_8$ , and  $Bi_8$  clusters in wedge and dimer configurations. All calculations are done in LDA; other parameters are as stated in Table III.

	$As_8$	$Sb_8$	$Bi_8$
$E_{\text{dim}}$	-39.362	-33.961	-31.883
$E_{\text{wedge}}$	-39.453	-34.961	-31.977
$E_{\text{dim}} - E_{\text{wedge}}$	0.091	0.219	0.095

structure is always more stable in these compounds (cf. Table IV).

Although both structures are very similar in energy in all systems, the transition from one structure to the other is very unlikely. In fact, due to the different symmetries the energy barrier between the structures is very high. Following the direct process proposed by Chen *et al.* [17], the pathway passes an intermediate state leading to a two barrier transition, with both barriers being at least 2 eV high.

The work of Janoschek [21] in 1992 corroborates our findings. He showed that in MP2 + ZPE no  $P_8$  cluster is more stable than two separated  $P_4$  clusters. If two  $P_4$  tetrahedron approach each other, the energy of the two-cluster system will drop slightly indicating that the dimer structure is in fact lower in energy than any other  $P_8$  cluster. In 1993 Kumar *et al.* reported [22,23] a new most stable isomer in the  $Sb_8$  system. They found the same dimer cluster we found for the  $P_8$  cluster. However, in our calculations of the  $Sb_8$  cluster we could not reproduce the dimer configuration as the most stable isomer neither in LDA nor in PBE.

Although the long bond between two  $P_4$  clusters may not be described well in DFT, it is clear that this structure is more stable than all previously found structures in DFT, showing that our method can quickly discover new minima in a given phase space.

## V. SUMMARY

We have proposed an optimization scheme based on the nudged-elastic-band (NEB) method. Contrary to the initial intention of the method, we do not search for saddle points but for stable minima. Our scheme can overcome local minima by the NEB's particular distribution of images along the band. The real forces tangential to the band are replaced by an artificial spring force that moves the images through the phase space without being hindered by potential barriers along the way. At the same time the images relax along the real potential perpendicular to the band. Local minima can be escaped from by adding and removing images in the band systematically. This enforces continual dynamics along the band, while relaxing toward the global minimum perpendicular to the band remains undisturbed. The method complements energy-based schemes, such as simulated annealing and the genetic algorithm. Our method is force based and the probability of an image escaping from a local minimum does not depend on the depth of the minimum but on its attractor width. Metastable states can then be found. We showed that our method finds the well-known most stable isomer of  $P_4$  and a new most stable isomer in the  $P_8$  system. The method has also been successfully

applied to the corresponding clusters of arsenic, antimony, and bismuth and can be applied to any generic optimization problem, as long as the phase space is continuous or can be continuously interpolated. For simplicity we manipulated the band by hand between the NEB runs, but for other systems it is possibly advantageous to automatize the proposed scheme.

#### ACKNOWLEDGMENTS

The DFT calculations have been performed on the supercomputer JUROPA at the Jülich Supercomputing Center with a grant from the FZ-Jülich. The authors are very grateful to R. O. Jones for supporting this work with his expertise in helpful discussions.

- 
- [1] N. Metropolis, A. W. Rosenbluth, M. N. Rosenbluth, A. H. Teller, and E. J. Teller, *J. Chem. Phys.* **21**, 1087 (1953).
- [2] A. S. Fraser, *Aust. J. Biol. Sci.* **10**, 484 (1957).
- [3] R. O. Jones and D. J. Hohl, *J. Chem. Phys.* **92**, 6710 (1990).
- [4] S. Hwang and R. Smith, *Korean J. Chem. Eng.* **29**, 25 (2012).
- [5] C. C. Queirolo, L. Silva, O. R. P. Bellon, and M. P. Segundo, *IEEE Trans. Pattern Anal. Mach. Intell.* **32**, 206 (2010).
- [6] S.-H. Yanga, J. Srinivasa, S. Mohana, D.-M. Leea, and S. Balajib, *J. Mater. Process. Technol.* **209**, 4471 (2009).
- [7] A. Tabatabaenejad and M. Moghaddam, *IEEE Trans. Geosci. Remote Sens.* **47**, 2035 (2009).
- [8] A. D. Stivala, P. J. Stuckey, and A. I. Wirth, *BMC Bioinformatics* **11**, 446 (2010).
- [9] J. S. Liu, A. J. Caley, A. J. Waddie, and M. R. Taghizadeh, *Appl. Opt.* **47**, 807 (2008).
- [10] X. Zhou, J. Zhao, X. Chen, and W. Lu, *Phys. Rev. A* **72**, 053203 (2005).
- [11] G. H. Jóhannesson, T. Bligaard, A. V. Ruban, H. L. Skriver, K. W. Jacobsen, and J. K. Nørskov, *Phys. Rev. Lett.* **88**, 255506 (2002).
- [12] W. Cheah and M. W. Finnis, *J. Mater. Sci.* **47**, 1631 (2012).
- [13] D. Sheppard, R. Terrell, and G. Henkelman, *J. Chem. Phys.* **128**, 134106 (2008).
- [14] G. Henkelman, G. Jóhannesson, and H. Jónsson, in *Theoretical Methods in Condensed Phase Chemistry*, edited by S. D. Schwartz (Kluwer Academic Press, New York, 2002), pp. 269–300.
- [15] G. Henkelman and H. J. Jónsson, *J. Chem. Phys.* **113**, 9978 (2000).
- [16] G. Seifert and R. O. Jones, *Z. Phys. D* **26**, 349 (1993).
- [17] M. D. Chen, R. B. Huang, L. S. Zheng, and C. T. Au, *J. Mol. Struct., Theochem* **499**, 195 (2000).
- [18] M. D. Chen, J. T. Li, R. B. Huang, L. S. Zheng, and C. T. Au, *Chem. Phys. Lett.* **305**, 439 (1999).
- [19] B. M. Gimarc and S. Warren, *Inorg. Chem.* **32**, 1850 (1992).
- [20] A. Kokalj, *Comput. Mater. Sci.* **28**, 155 (2003). Code available from [<http://www.xcrysden.org/>].
- [21] R. Janoschek, *Chem. Ber.* **125**, 2687 (1992).
- [22] V. Kumar, *Phys. Rev. B* **48**, 8470 (1993).
- [23] V. Sundararajan and V. Kumar, *J. Chem. Phys.* **102**, 9631 (1995).